C. R. Physique 13 (2012) 268–279

Contents lists available at SciVerse ScienceDirect

Comptes Rendus Physique

www.sciencedirect.com

Use of large scale facilities for research in metallurgy

Following individual grains during solid-state phase transformations with 3DXRD microscopy

Suivi de grains individuels lors de transformations de phases à l'état solide par microscopie 3DXRD

S. Eric Offerman *, Hemant Sharma

Department of Materials Science and Engineering, Delft University of Technology, Mekelweg 2, 2628 CD, Delft, The Netherlands

ARTICLE INFO

Article history:
Available online 30 January 2012

Keywords:
3DXRD
Microstructure
ESRF

Mots-clés :
3DXRD
Microstructure
ESRF

ABSTRACT

The mechanical properties of metals strongly depend on the microstructure, which is formed during their production and processing. Understanding the underlying mechanisms of the nucleation and growth kinetics during solid-state phase transformations in steel is of vital importance to control its microstructure. The kinetics of individual grains in the bulk of steel can be measured *in situ* with the three-dimensional X-ray diffraction microscopy (3DXRD) at the European synchrotron radiation facility (ESRF). Simultaneously the fraction transformed, the nucleation rate, and the growth rate of individual grains can be measured. Unique *in situ* measurements of nucleation and growth rates of individual austenite and ferrite grains are presented.

RÉSUMÉ

Les propriétés mécaniques des métaux dépendent fortement de leur microstructure, qui est formée lors de leur production et procédés. La compréhension des mécanismes complexes sous-jacents aux cinétiques de germination et croissance lors de transformations de phases à l'état solide dans les aciers est d'une importance vitale pour contrôler leurs microstructures. La cinétique de formation de grains individuels dans le volume d'un acier peut être mesurée *in situ* grâce à la microscopie tri-dimensionnelle à diffraction de rayons X (3DXRD) au synchrotron européen ESRF. Cette technique permet de mesurer simultanément la fraction transformée, le taux de germination et la vitesse de croissance de grains individuels. Nous présentons dans cet article des mesures uniques de taux de germination et de croissance de grains individuels d'austénite et de ferrite.

1. Introduction

Processes involving grain nucleation and growth are ubiquitous in materials science. Nevertheless, at the present time, experimental studies of the underlying mechanisms involved in these processes is extremely challenging. Herein, we describe these difficulties and introduce some examples of experiments carried out using three-dimensional X-ray diffraction

* Corresponding author.
E-mail address: S.E.Offerman@tudelft.nl (S.E. Offerman).

1631-0705/$ – see front matter
doi:10.1016/j.crhy.2011.12.002

(3DXRD) technique, developed jointly by scientists from metals in 4D group in Risø National Laboratory, Denmark and beamline ID11 at European Synchrotron Radiation Facility (ESRF), France. We focus on solid-state phase transformations in steel, which is an important metallurgical process.

For solid-state phase transformations, the experimental difficulty stems from several facts. The critical nuclei are very small (in the range of nanometers) and exist as nuclei only for a short time before they grow into larger grains. These nuclei often form at defects or interfaces in the bulk of the material. From classical nucleation theory, it is known that the energies of the grain boundaries between the parent grains as well as between the parent and nucleating grains are very important. To determine the energies of these interfaces, the local atomic arrangement and chemistry must be known, which requires a local probe with atomic resolution. At the same time, a large volume of the material needs to be probed in order to obtain sufficient statistics about the different types of potential nucleation sites available in the heterogeneous microstructure of the alloy. Moreover, for accurate measurements, the grain-boundary energy between parent grains should be obtained before the nucleus forms, and the energy of the interface between the nucleus and the matrix should be determined at the moment of formation of a critical nucleus.

Notwithstanding the great improvements and sophistication in experimental techniques, no technique is currently available that simultaneously fulfills all of the requirements just described. As a result, studies of nucleation during solid-state phase transformations have been limited to either high-spatial-resolution measurements with instruments such as high-resolution electron microscopes [1,2] and/or 3D atom-probe microscopes [2–4] or measurements in which large volumes of the material are investigated with optical and electron microscopy and electron back scatter diffraction (EBSD) [5–7]. Such techniques are at best limited to a series of ex situ measurements on different specimens with inherently different parent microstructures. Hence, only statistical information on average behavior can be obtained.

The recent development of the 3DXRD microscope at beamline ID11 of the ESRF promises a new perspective for studies of the microstructural evolution in materials in general. Although the technique does not currently fulfill all of the requirements just discussed, important steps have been made for *in situ* measurements in the bulk of optically opaque materials with (sub)micron resolution. The 3DXRD method has been used for a range of applications including studies of plastic deformation, rotation of grain orientation, stability of nanocrystalline materials, solidification, grain maps, domain switching, and crystal structure determination for materials as diverse as metals, ceramics, and even pharmaceutical compounds.

2. 3DXRD microscopy

2.1. Introduction

3DXRD microscopy is a 3D X-ray imaging technique applicable to polycrystalline specimens, with a setup rather similar to that of X-ray tomography. The difference is that, in tomography, one probes the attenuation of the direct beam and reconstructs the density within the sample. In 3DXRD, one probes the intensity of individual diffraction spots arising from individual grains in the material. This allows mapping of the 3D structure (i.e., the crystallographic orientation; shape; and x, y, z position of each grain in the probed volume) of polycrystalline samples. 3DXRD also provides information on the local stress state and the local phase (atomic structure). In addition, the high brilliance of third-generation synchrotron radiation facilities makes it possible to follow the change in intensity of individual diffraction spots as a function of time. As will be shown later this makes it possible to probe the growth kinetics of individual grains inside the material as a function of processing conditions of the material. A variant of 3DXRD, called Diffraction Contrast Tomography (DCT) [8] is also available with better spatial resolution.

3DXRD microscopy can be performed only at synchrotron radiation sources because a high-intensity source is needed to obtain a sufficient signal-to-noise ratio. The first 3DXRD instrument was installed at ESRF and is sketched in Fig. 1. To ensure a high penetration depth (e.g., 5 mm in steel and 4 cm in Al), the sample is illuminated by a monochromatic high-energy (50–100 keV) X-ray beam. The sample is mounted on an ω-rotation stage, where ω is the rotation about an axis perpendicular to the incoming beam. Grains, cells, nuclei, and so on within the illuminated sample volume that fulfill the Bragg condition will generate a diffracted beam, which is recorded on a 2D detector. To probe the complete sample structure within the gauge volume and not just the parts that fulfill the Bragg condition, the sample is rotated in ω. Essential to the 3DXRD technique for probing the three-dimensional microstructure is the idea of mimicking a 3D detector by positioning several 2D detectors at different distances from the center of rotation and exposing these detectors either simultaneously (as many detectors are semitransparent to hard X-rays) or sequentially. For more information regarding the measurement of 3D microstructures, the reader is referred to Refs. [9–14].

The 3DXRD methodology involves a compromise between spatial and temporal resolution. To optimize performance for a given study, the microscope can be run in several modes [14]. In “slow mode,” complete 3D maps of the crystallographic orientations are provided with a mapping precision of 5 μm × 5 μm × 1 μm, but with a low time resolution on the order of a few hours for a map of about 1000 grains. On the other hand, in “fast mode,” hundreds of grains can be monitored simultaneously with a time resolution on the order of seconds, for grains as small as 20 nm. In this mode, however, only the change in the volume, orientation, or strain of each grain can be measured, but not the grain shape. In general, the more information is acquired simultaneously from the material, the longer the measurement time. In this paper we focus on the fast mode of 3DXRD that allows studying *in situ* the phase transformation kinetics of individual grains.

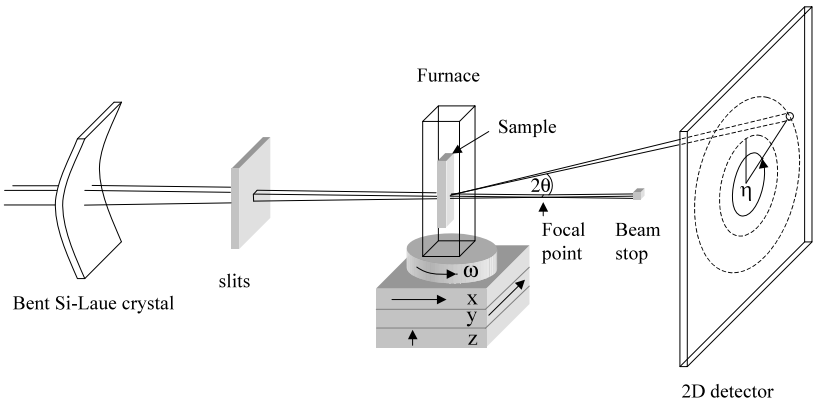

Fig. 1. Schematic drawing of the experimental set-up for the 3DXRD measurements. The set-up consists of a bent Si-Laue crystal, slits, and a 2D detector. The specimen is positioned in a furnace, which is mounted on a table that can be translated and rotated. Image taken from Ref. [17].

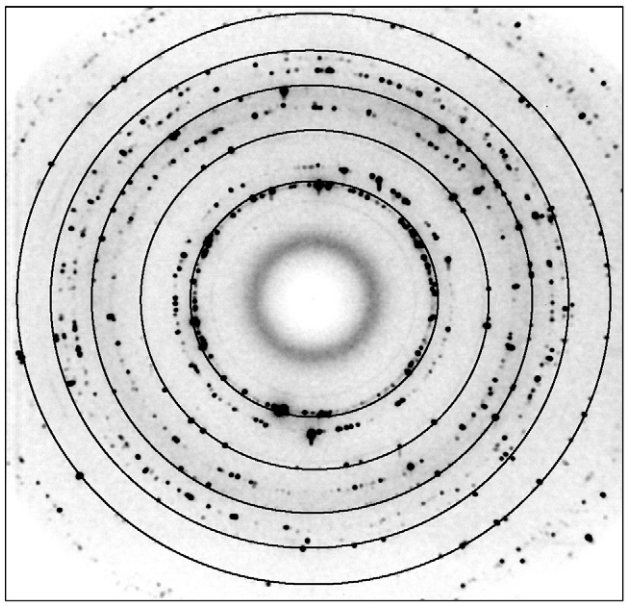

Fig. 2. X-ray diffraction pattern of steel showing the separate austenite and ferrite reflections at 763 °C. The solid rings indicate the expected scattering angles from the ferrite grains illuminated by the X-ray beam. From the inside towards the outside the following *hkl* diffraction rings are completely with the range of the detector: γ_{111}, α_{110} (close to γ_{111}), γ_{200}, α_{200}, γ_{220}, α_{211}, γ_{311}, γ_{222}, α_{220}, α_{310}, γ_{400} (close to α_{310}). Image taken from Ref. [18].

2.2. Experimental method 3DXRD

The 3DXRD microscope used for this study is located at beamline ID11 of the European Synchrotron Radiation Facility (ESRF). Fig. 1 shows a schematic drawing of the experimental set-up as it was used to study the phase transformation kinetics of individual grains described in this paper. A white synchrotron beam diffracts from a bent silicon Laue crystal, which gives a monochromatic (80 keV), vertically focused X-ray beam. Two sets of vertical and horizontal slits define the beam size at the sample, which is typically 100×100 μm^2. In order to illuminate the sample uniformly, a homogeneous flux of photons is needed over the whole cross-section of the beam. The sample is positioned out of focus. In this way the beam size can be altered with the slits during the experiment. The sample was placed in a specially designed furnace [15], which allowed the *in situ* study of the austenite–ferrite and ferrite–austenite transformation in steel by X-ray diffraction. The furnace is positioned on a table, which can be translated in three directions (x, y, z) and rotated over an angle ω (see Fig. 1). The diffracted X-rays are recorded with a 2D-detector (FReLoN CCD camera [16]).

Separate diffraction spots appear on the recorded diffraction pattern, an example of which is shown in Fig. 2. The detection of separate reflections is achieved by choosing a relatively small beam size of about 5 times the maximum size of the grains in the material under investigation. As a result a limited number of grains contribute to the diffraction pattern. Each diffraction spot on the detector corresponds to a single grain in the material. The typical recording time of a diffraction pattern is of the order of 1 s. The complete Bragg intensity of an individual grain is recorded by slightly rotating the sample

about the z-axis (see Fig. 1) over an angle $\Delta\omega$. This way, around 200 spots are followed during the experiments. The details of theory of 3DXRD and data analysis procedure can be found elsewhere [17,19].

3. Nucleation theory

Here we give a brief background of the nucleation theory and the Ψ-parameter which will come later in Section 4. The change in Gibbs free energy ΔG during heterogeneous nucleation of a volume V of ferrite on austenite grain boundaries, edges, or corners is given by [20]:

$$\Delta G = -V(\Delta G_V - G_S) + \sum_i A_i \sigma_i \tag{1}$$

where ΔG_V is the difference in Gibbs free energy per unit volume between ferrite and austenite. ΔG_V is also known as the driving force for nucleation and depends on the chemical composition and temperature. The misfit strain energy, G_S, effectively reduces ΔG_V but is usually neglected, as was also the case in the results presented in Section 4. The removal of an area $A_{\gamma\gamma}$ of the austenite/austenite grain boundary with grain boundary energy $\sigma_{\gamma\gamma}$ results in the reduction of the Gibbs free energy by $A_{\gamma\gamma}\sigma_{\gamma\gamma}$. The creation of an area $A_{\alpha\gamma}$ of ferrite/austenite interface with interface energy $\sigma_{\alpha\gamma}$ results in an increase of the Gibbs free energy by $A_{\alpha\gamma}\sigma_{\alpha\gamma}$. The index i represents all the interfaces that play a role during nucleation. In the summation, the terms for disappearing interfaces are taken negative.

The nucleus volume can be given as $z_V R^3$ where z_V is a geometrical parameter depending on the shape of the nucleus and R is the nucleus dimension. The interfacial area is given by $z_A^i R^2$, where z_A^i is a geometrical parameter depending on the shape of the ith interface. The size R^* of the critical nucleus is defined by the position of maximum in ΔG as a function of R, and is thus given by

$$R^* = \frac{2\sum_i z_A^i \sigma_i}{3 z_V \Delta G_V} \tag{2}$$

The corresponding activation energy for nucleation ΔG^* is given by

$$\Delta G^* = \frac{4}{27}\frac{(\sum_i z_A^i \sigma_i)^3}{z_V^2 \Delta G_V^2} \equiv \frac{\Psi}{\Delta G_V^2} \tag{3}$$

with

$$\Psi = \frac{4}{27 z_V^2}\left(\sum_i z_A^i \sigma_i\right)^3 \tag{4}$$

Eqs. (3) and (4) are valid for every shape of the critical nucleus. Eq. (4) contains all the information about the shape of the nucleus and the interfacial energies that are involved in nucleation. Eqs. (3) and (4) show that the balance between the energy required for the formation of new interfaces and the energy released due to the removal of old interfaces is represented by the parameter Ψ.

In Eq. (4), interface energy is present as a power of three, which means that the correct knowledge of interface energy is very important for calculation of the Ψ parameter. Although attempts have been made to calculate the interface energy for pure iron at 912 °C (temperature at which both ferrite and austenite are in equilibrium) [21] it is still not possible to calculate the interfacial energy for alloyed systems as a function of temperature and local composition.

4. Examples: Solid-state nucleation and grain growth during phase transformations

Understanding the underlying mechanisms of grain nucleation and growth during solid-state phase transformations is of utmost importance for predicting the evolution of the microstructure and, therefore, the final mechanical properties of many polycrystalline materials; we focus the discussion here on steel. The inhomogeneous nature of microstructures in steel requires simultaneous measurements of many parameters influencing grain nucleation and growth in the bulk of the material in real time and locally on a microscopic-feature scale [22].

4.1. Austenite to ferrite transformation

4.1.1. 3DXRD measurements and nucleation modeling

3DXRD in the fast mode enables *in situ* determination of bulk nucleation rates per unit untransformed volume. Such measurements can be performed by simultaneously counting the number of individual diffraction spots associated with the relevant phase and measuring the fraction transformed. As only small rotation ranges are required, the time resolution is typically in the range of seconds to minutes. As an example, we first present results for a medium carbon steel (0.21 wt% C, 0.51 wt% Mn and 0.20 wt% Si) slowly cooled from 1173 K (with the high-temperature austenite phase) to 873 K (with the low temperature ferrite phase) at a 5 K/min cooling rate [18,23–26], using the furnace described in Ref. [15]. The energy

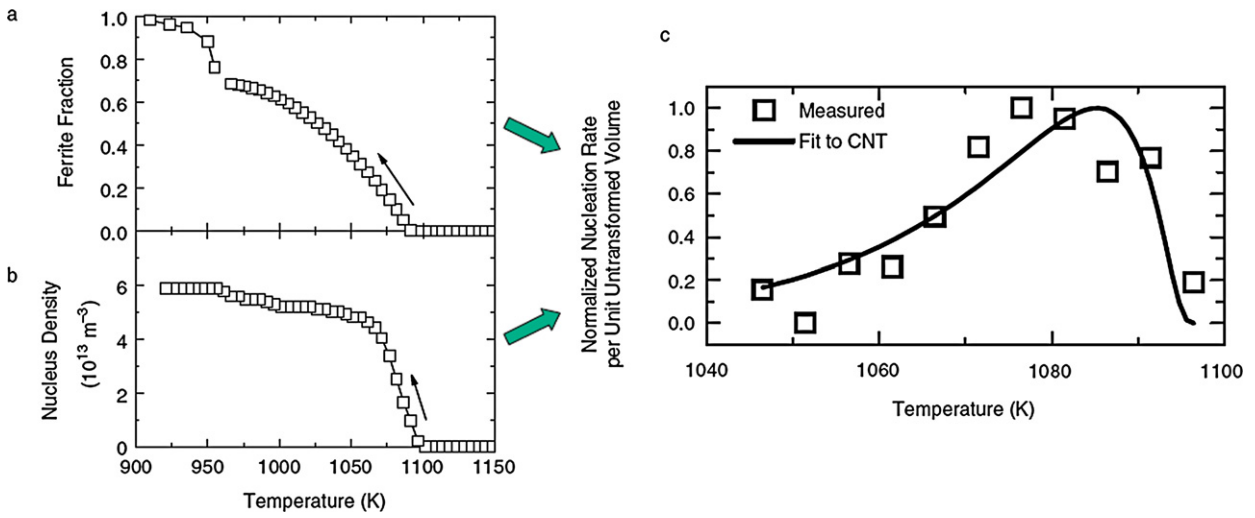

Fig. 3. Results from 3DXRD measurements during austenite-to-ferrite phase transformation in medium carbon steel that was slowly cooled from 1173 K to 873 K at a rate of 5 K/min: (a) ferrite fraction, (b) ferrite nucleus density, and (c) derived ferrite nucleation rate per unit untransformed volume. The measured nucleation rate was fitted to the classical nucleation theory (CNT, solid line) to obtain the critical nucleus parameters. Data from Refs. [18,23,26]. Image taken from Ref. [29].

of the monochromatic X-rays corresponds to 80 keV, the beam size to 94×97 μm^2, and the thickness of the sample to 400 μm. During the exposure, the sample is continuously rotated around the vertical axis over an angle from $-0.8°$ to $0.8°$. In order to verify if a diffraction spot is valid, we took additional exposures for rotation angles from $-2.4°$ to $-0.8°$ and from $0.8°$ to $2.4°$, which tell us whether the complete integrated intensity is observed in the central exposure. Once every six exposures the beam size was expanded to 139×139 μm^2 in order to check whether the total volume of the grain is illuminated by the small central beam. The data analysis was carried out according to the procedure given in Refs. [17,19]. Figs. 3a and 3b show the simultaneously measured ferrite fraction and ferrite nucleus density. The ferrite nucleus density was determined by counting the number of spots on the detector during the transformation [25]. From Figs. 3a and 3b, the normalized nucleation rate per unit untransformed volume was determined, as shown in Fig. 3c. A high time resolution was obtained in this experiment by rotating the specimen over a small angle. As a result, a limited but sufficient number of ferrite nuclei are in reflection configurations, which allows the estimation of the nucleus density because the observed ferrite texture after the transformation was random (although the absolute nucleus density is not required for Fig. 3c). All ferrite nuclei in the volume of interest can be determined directly by rotating the specimen over a larger angle, at the cost of the time resolution. With the experimental settings, the signal-to-noise ratio in the images implies that the "nuclei" were first observed at the moment that their size (i.e., radius) was above 2 μm. Nevertheless, the nucleation rate can still be deduced from the measurements because the 3DXRD measurements also reveal the volume of the individual grains as a function of time (see Fig. 4), which was found to be linear at the early stage of growth. The observed growth behavior at the early stage is in agreement with synchrotron measurements on nanocrystalline grains of iron [27]. This implies that the time difference between the moment at which the grain acquires a radius of 2 μm and that at which the critical nucleus (of a few nanometers) has formed is negligible. More details on the experiments can be found in Refs. [18] and [28].

Interpretation of the measured nucleation rate in terms of classical nucleation theory (Fig. 3c) shows that the activation energy for ferrite nucleation in steel is much lower than expected on the basis of previous schematic models of the nucleus morphology and grain-boundary energies [30]. In the present case, the activation energy for ferrite nucleation is even as low as $2kT$, which is close to the average thermal energy of the atoms. This means that ferrite nucleation rates in steel can be very high. The value of Ψ parameter, explained in Section 3, can be derived by fitting the measured nucleation rate with classical nucleation theory. In this case, the value of Ψ is found to be $\Psi = 5 \times 10^{-8}$ J^3/m^6. Other models, such as Clemm and Fisher model [31] and the pillbox model from Lange et al. [32] yield values of Ψ equal to $\Psi_{CF} = 7.1 \times 10^{-2}$ J^3/m^6 and $\Psi_{LEA} = 2.1 \times 10^{-6}$ J^3/m^6, respectively. This shows that the value of Ψ obtained for the *in situ* synchrotron experiments is at least two orders of magnitude lower than what other models predict.

4.1.2. Grain growth

The 3DXRD microscope is also unique in enabling *in situ* studies of the change in volume of individual bulk grains during a transformation. In the same study of medium carbon steel as discussed in the previous section, the individual grain volumes were derived from the change in integrated intensity of the associated diffraction spots [33]. Figs. 4a–4d (top) show the growth curves of individual ferrite grains during the austenite-to-ferrite transformation [18]. Fig. 4a (top) shows that, initially, the growth rate is described by the well-established theory of Zener [34] for diffusion-controlled growth (dashed line). At a later stage, the curves start to deviate from the Zener theory as a result of the overlap of diffusion fields. A simplified model was developed in by Offerman et al. [23] to include the effects of overlapping diffusion fields on the growth of ferrite grains (solid lines in Fig. 4). For details about the model, the reader is directed to Ref. [23].

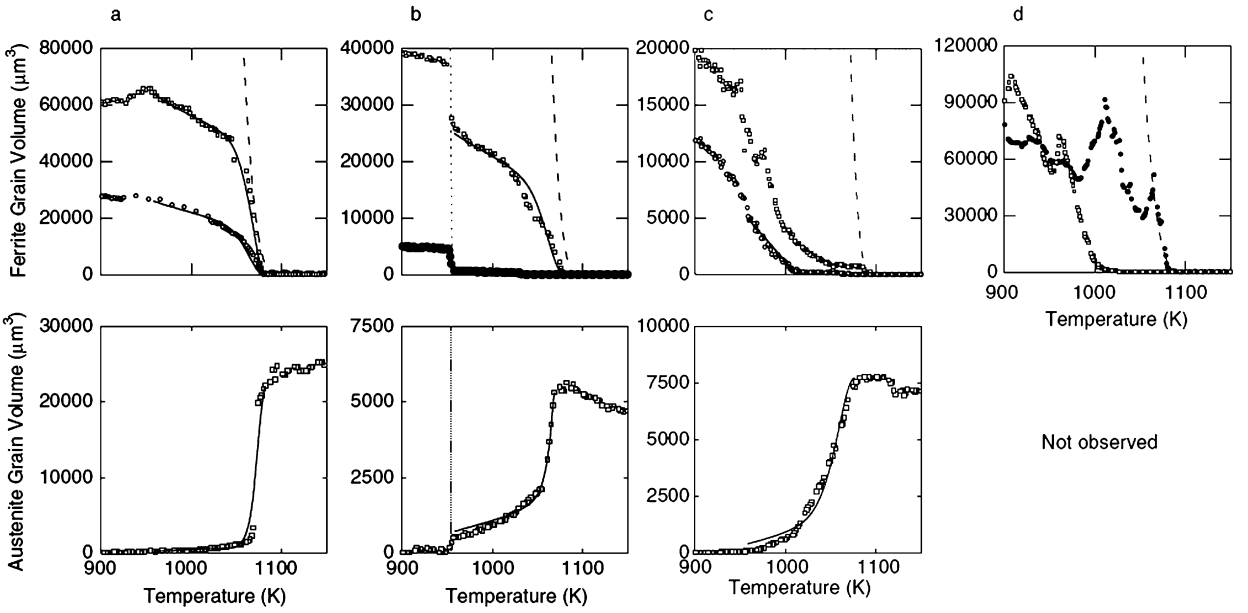

Fig. 4. Results from 3DXRD measurements during austenite-to-ferrite phase transformation in medium carbon steel that was slowly cooled from 1173 K to 873 K at a rate of 5 K/min. Figures (a)–(d) (top) show four representative types of growth curves in eight individual ferrite grains: (a) ferrite grows according to the Zener theory (dashed line) during the early stages, and at the later stages, soft impingement of diffusion fields decreases the growth rate (the solid line represents a model that takes into account the overlap of diffusion fields; see Ref. [23]); (b) ferrite grows as in part a but continues to grow in pearlite; (c) retarded nucleation and growth of ferrite occurs in caron-enriched areas; and (d) ferrite growth and temporary shrinkage occurs as a result of the combined effects of growth due to the phase transformation and shrinkage due to hard impingement of ferrite grains. In (a)–(c) (bottom), the tree types of corresponding austenite decomposition are shown for three individual austenite grains. Note: The ferrite and austenite grains that are shown are not one-to-one related to each other. Data taken from Refs. [18] and [23]. Image taken from Ref. [29].

Fig. 4 reveals three other types of ferrite grain growth in steel: grains that continue to grow into pearlitic ferrite, meaning ferrite that is part of a pearlite colony consisting of two interpenetrating single crystals of ferrite and cementite (Fe_3C) that are locally ordered as alternating plates but that are connected in the third dimension (Fig. 4b, top); grains that nucleate and grow in the (overlapping) diffusion fields of other grains (Fig. 4c, top); and grains that grow, temporarily shrink, and grow again (Fig. 4d, top). The latter type of ferrite growth is ascribed to the simultaneous growth as a result of the phase transformation and hard impingement with neighboring grains, in which the ferrite/ferrite interface is "pushed back" into the ferrite grain. Additional evidence for this hypothesis is found by examining the decomposition of individual austenite grains, which shows that the first three types of ferrite grain growth curves have corresponding mirror images of the austenite grain growth curves, as shown in Figs. 4a–4c (bottom). However, for the last type of ferrite grain growth, a corresponding mirror image is not found in the austenite, which strongly suggests that the oscillatory ferrite growth is not the result of a back-transformation.

4.1.3. Comparing different steel compositions

Fig. 5 shows the measured ferrite fraction as a function of temperature during continuous cooling from 1173 K to 873 K at a rate of 5 K/min for three steels with different compositions (C22 – 0.214 wt% C, C35 – 0.364 wt% C and C45 – 0.468 wt% C, see Ref. [28] for detailed compositions). The austenite/pearlite transformation starts at approximately the same temperature of 685 °C for all the three steel grades.

Fig. 6 shows the ferrite nucleus density as a function of temperature during continuous cooling for the three steel compositions. The ferrite nucleus density is seen to increase rapidly in the initial stage of the phase transformation, after which the nucleus density continues to increase more gradually over a considerable temperature range. The ferrite nucleus density depends on the number of potential number of ferrite nucleation sites. This is related to the austenite grain size distribution, the shape of the austenite grains, the grain boundary energy of the austenite grains, and the energy of the austenite/ferrite interfaces.

The ferrite nucleation rate is determined by taking the derivative of the ferrite nucleus density. Fig. 7 shows the measured ferrite nucleation rate normalized to the maximum nucleation rate as a function of temperature during continuous cooling for the three steel compositions. In Fig. 7, the measured nucleation rate is compared to the classical nucleation theory (see Ref. [28] for details). The solid lines are calculated without fitting parameters according to the classical nucleation theory, and agree very satisfactorily to the normalized nucleation rates that are measured. In agreement with the findings of Huang and Hillert [35], we observe that most of the nuclei form during the formation of the first 10–30% of ferrite fraction.

Again, classical nucleation theory was used to fit the nucleation data obtained for the three different alloys (Fig. 13). The best fit was obtained with a value of Ψ equal to $\Psi = 5 \times 10^{-8}$ J^3/m^6, derived in Section 4.1.1.

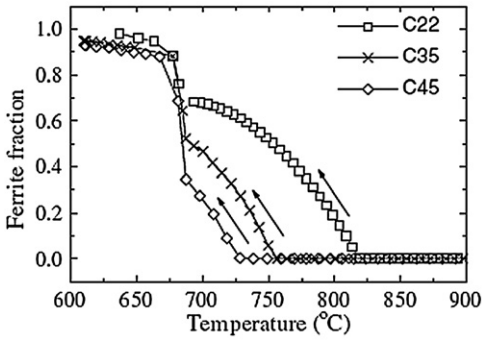

Fig. 5. The measured ferrite fraction as a function of temperature during continuous cooling from 900 °C to 600 °C at a rate of 5 °C/min for the three steel compositions. Figure taken from Ref. [28].

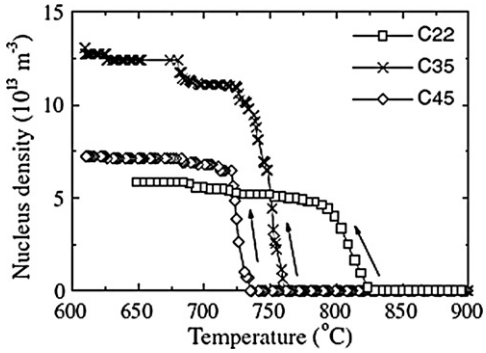

Fig. 6. Ferrite nucleus density as a function of temperature during continuous cooling from 900 °C to 600 °C at a rate of 5 °C/min for the three steel compositions. Figure taken from Ref. [28].

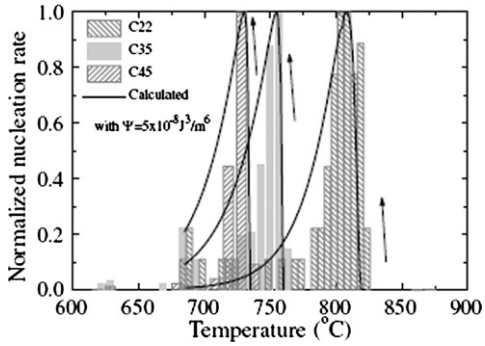

Fig. 7. Ferrite nucleation rate as a function of temperature during continuous cooling from 900 °C to 600 °C at a rate of 5 °C/min for the three steel compositions. The ferrite nucleation rate is scaled to the maximum in the experimental nucleation rate. For more details about the solid lines, see text. Figure taken from Ref. [28].

4.2. Ferrite/pearlite-to-austenite transformation

So far, the interest in understanding nucleation and growth of austenite during formation from an initial microstructure of ferrite and pearlite attracted limited attention, but the interest is continuously increasing due to the development of new types of steels like dual-phase steel and transformation induced plasticity (TRIP) steel. As is the case with austenite-to-ferrite transformation, 3DXRD is a very valuable tool in this case as well, due to the ability to carry out *in situ* experiments. As an example, we present a case of two alloys, C22 and C35 (see Ref. [28] for chemical composition). The alloys are heated in the furnace described in Ref. [15] at a heating rate of 10 °C/min to a final temperature of 900 °C. Experimental details can be found in Ref. [28]. The beam size used is 63×70 μm^2 and every sixth exposure the beam is expanded to 90×90 μm^2. The sample is rotated over an angle $\Delta\omega$ of 0.5° to get a sufficient number of grains into reflection. In order to make sure that a diffraction spot is valid, additional exposures are taken during rotation over small angles 0.5° just before and after the central rotation. To determine the temperature during the experiments, a thermocouple was placed under the sample in close vicinity to it, but not in contact with it. This gives rise to a difference in the temperature of sample and the measured

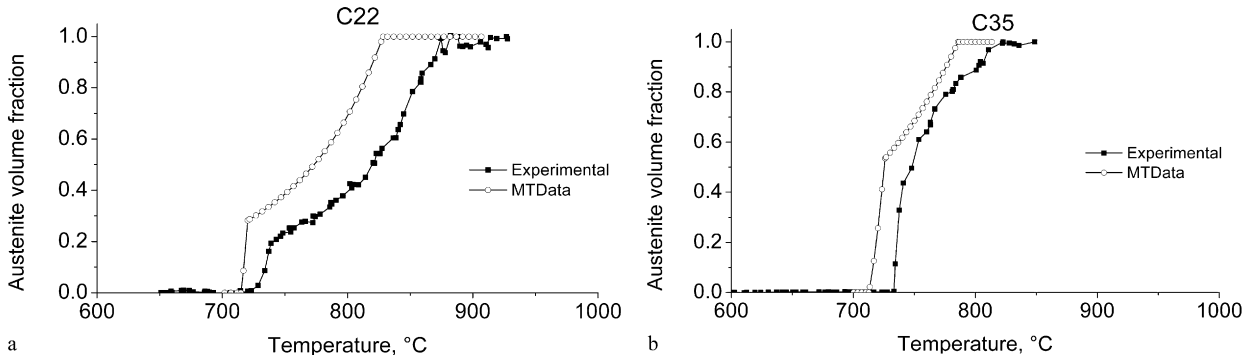

Fig. 8. Austenite volume fraction as measured by 3DXRD (solid rectangles) and calculated using MTData® (open circles) for (a) C22 and (b) C35 alloys. Figure taken from Ref. [36].

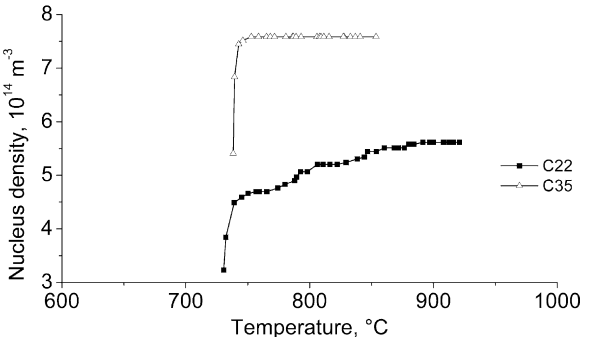

Fig. 9. Austenite nucleus density as the function of temperature for C22 (solid rectangles) and C35 (open triangles) alloys. Figure taken from Ref. [36].

temperature. In order to calibrate the temperature measurement obtained during the experiments, additional dilatometric measurements were made. The temperature recorded during 3DXRD experiments was then shifted to match the start of transformation recorded from dilatometric measurements and from 3DXRD experiments.

Figs. 8a and 8b show the measured volume fraction for the C22 and C35 alloys as a function of temperature as compared to the para-equilibrium fraction as obtained from MTData® [37]. There are remarkable similarities in the curves shown in Fig. 8. All the curves initially show a fast increase in the austenite volume fraction, corresponding to the pearlite-to-austenite transformation [38,39]. It is then followed by a slower increase in austenite fraction, corresponding to the ferrite-to-austenite transformation. The slower increase in austenite volume fraction in ferrite is due to the lower carbon content of ferrite, which makes austenite less stable.

4.2.1. Nucleation

Fig. 9 shows the measured nucleus density for C22 and C35 alloys as a function of temperature during continuous heating to the one-phase region. Two different stages in the nucleation behavior are observed. Just after the beginning of the pearlite/ferrite-to-austenite transformation, there is a very fast increase in the number of austenite grains. Pearlite–ferrite (or pearlite–pearlite) grain boundaries are the most favorable places for austenite nucleation for two reasons: the presence of the incoherent high-energy interface stimulates heterogeneous nucleation, and the availability of carbon makes the newly formed nuclei stable. The higher amount of pearlite in C35 alloy is responsible for the higher ferrite nucleus density than in C22 alloy.

For the C22 alloy, after the first stage of very sharp increase, in the second stage of transformation, when nucleation at ferrite–ferrite grain boundaries takes place, the nucleus density continues to increase, forming about 25% of the total number of nuclei. However, for the C34 alloy, no new nuclei appear to form, meaning that the transformation proceeds further via the growth of already existing austenite grains into pro-eutectoid ferrite.

Further analysis of nucleation data obtained from C22 alloy is carried out in terms of classical nucleation theory. The fraction of austenite nuclei formed on ferrite–ferrite grain boundaries is taken from the measured data (see Fig. 10). The driving force for nucleation is calculated from MTData® thermodynamic database through the parallel tangent construction assuming para-equilibrium condition. Fig. 10 shows that, except for the first several degrees, for most of the transformation range, the calculated activation energy for nucleation values are smaller than kT. The reason for the small activation energy for nucleation could be that the energy needed to form a new interface is largely compensated by the energy that is removed from the system by eliminating the grain boundary of the parent phase where nucleation takes place. The experimental nucleation data was fit by using classical nucleation theory and the best fit was obtained for $\Psi = 4.8 \pm 1.0 \times 10^{-8}$ J^3/m^6.

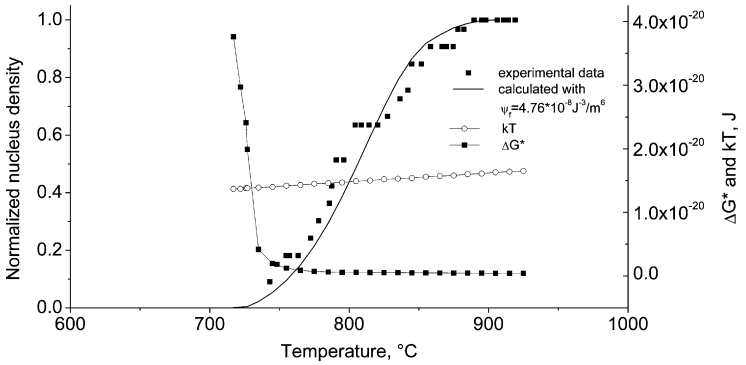

Fig. 10. Experimental and calculated values for the density of austenite nuclei on ferrite–ferrite grain boundaries, kT and ΔG^* values as a function of temperature for the C22 alloy. The ferrite nucleus density is scaled to the maximum in the experimental nucleation density. The solid line is a fit of the experimental data to the classical nucleation theory. Figure taken from Ref. [36].

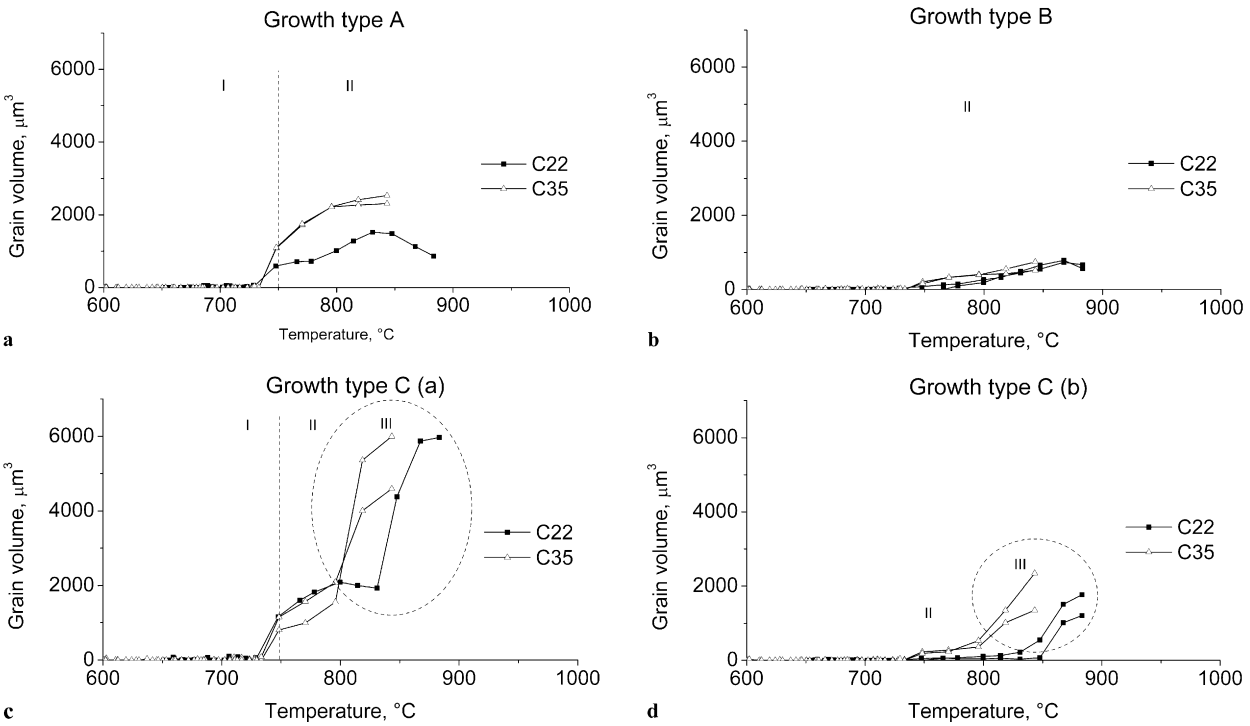

Fig. 11. Growth types (a) fast, possibly nucleated on pearlite–ferrite and (b) slow, possibly nucleated on ferrite–ferrite grain boundaries; (c) and (d) are similar to (a) and (b) respectively, but with a growth acceleration in the last stages of the transformation. Open triangles are for C35 and solid rectangles for C22 alloys. I, II, and III indicate different growth kinetics. Figure taken from Ref. [36].

This value of Ψ is of the similar order as the one obtained for nucleation of ferrite in austenite (Section 4.1) and much lower than model predictions. Such a low value gives information about the specific nucleation conditions, such as that nucleation takes place at sites that are high in energy (for example, triple edges and quadruple points) and that austenite nuclei form with relatively low interfacial energy.

4.2.2. Growth

Fig. 11 shows three types of austenite grain growth modes as observed during the experiments. Each individual growth type exhibits one or several of the following growth kinetics:

I. fast growth (austenite growth in pearlite);
II. slow growth (austenite growth in ferrite);
III. extremely fast growth (massive growth).

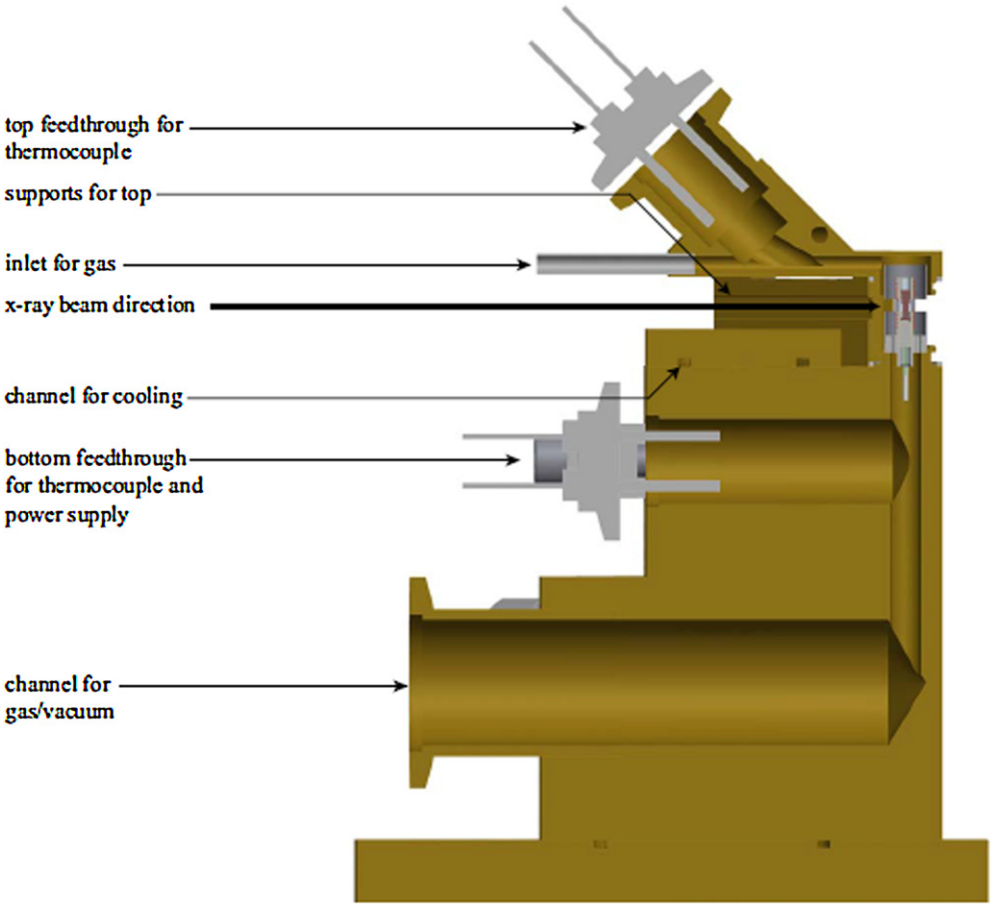

Fig. 12. Cut-out view of the 3DXRD furnace. Different parts of the furnace are indicated. One thermocouple is spot welded on top of the sample.

Growth type A (see Fig. 11a) is similar to the overall transformation curves (compare with Figs. 8a and 8b). Due to this similarity it is possible to suggest that the transformation starts with the fast growth of austenite grains into the pearlite colonies (growth kinetics I) and continues as a slow ferrite-to-austenite transformation (growth kinetics II). Growth type B (Fig. 11b) consists of only growth kinetics II, and is attributed to the nucleation and growth of new grains on the ferrite–ferrite grain boundaries. The peculiarity of growth type C (Figs. 11c and 11d) is that at the final stages of the transformation there is a strong acceleration of the process (growth kinetics III). The initial stages of growth are similar to growth types A and B growth from pearlite–ferrite grain boundaries (similar to growth type A, growth kinetics I, II) or from ferrite–ferrite grain boundaries (similar to the growth type B, growth kinetics I, II). However, the acceleration of the transformation at the last stage of the transformation is remarkable. A possible explanation of such behavior is a change in growth mode – from partitioning (below the T_0-temperature of the Fe–C system) to massive transformation (above T_0). In the latter type of transformation the original phase transforms to a new one with the same composition and the transformation proceeds rather fast, since the redistribution of elements (in this case carbon) is not necessary.

5. Outlook

The work described in this paper concerns 3DXRD-data taken by rotating the specimen over small angles of about 3 degrees. As a result, a selected number of grains come into reflection. This means that the nucleation and growth of a represented number of grains can be followed for materials with random texture. The development of the 3DXRD furnace [40], see Figs. 12 and 13, has opened up new possibilities for experiments, since the furnace opens the opportunity to rotate the specimen over 90 degrees (additional 90 degrees at the 'back' of the furnace). First, this means that all grains come into reflection and all growth curves of all grains in the illuminated volume can be studied. Second, the texture evolution during phase transformations at the level of individual grains can now also be studied. Third, the 3D-microstructure of materials can be measured at elevated temperatures. Fourth, complex industrial thermal heat treatments can be simulated in the furnace. Fifth, the furnace allows the possibility of combining kinetics measurements with 3-dimensional reconstruction of the microstructure (because of possibility of rotation of sample over 180° on opposite sides). Such data would not only shed light on the role of misorientations between grains on growth but also provide valuable information about the

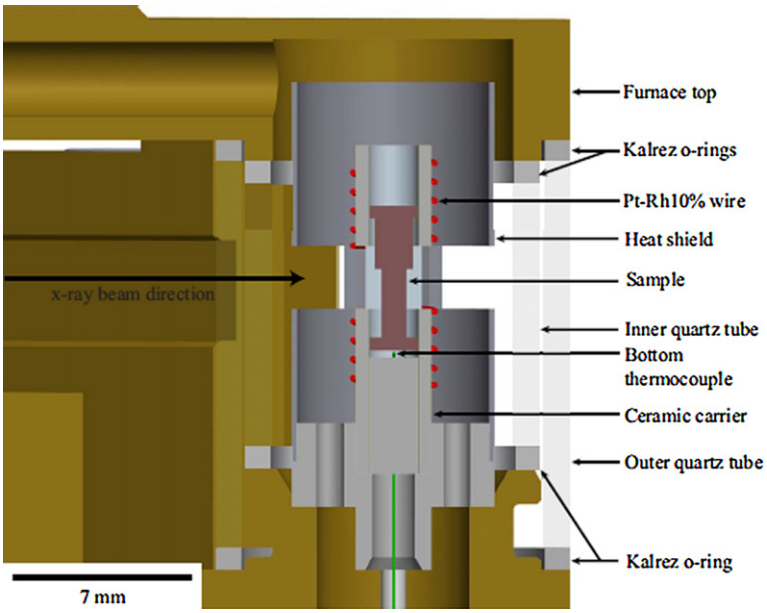

Fig. 13. Cut-out view of the specimen chamber. The X-ray beam direction and location of specimen are indicated. For changing the specimen, furnace top is removed, and the specimen is dropped onto the bottom thermocouple. Geometry of the specimen can be seen with the step due to change in diameter visible.

location of nucleation and type of interfaces favoring nucleation. In addition to that, the furnace also provides the ability to follow kinetics of all the grains inside the material. The experiments presented here were carried out using a beam size smaller than the horizontal sample dimension and using a single rotation angle to capture full integrated intensity from a grain in a single image. With availability of better optics and up gradation of beamline ID11 at the ESRF in combination with the 3DXRD furnace, it is now possible to uniformly illuminate full sample diameter, thus improving statistics and making data analysis better. The unique combination of ability to reach high temperatures and high rotation angles make it possible to study *in situ* texture evolution in materials.

Studying the formation of austenitic microstructures of construction steel in three-dimensions at elevated temperatures is now possible with the 3DXRD furnace. Such *in situ* measurements will contribute to our understanding of the evolution of metallic microstructures at elevated temperatures and open the opportunity to design the microstructure of steel at high temperatures, which is required for the development of advanced high-strength steel, fire-resistant steel for the construction sector, and steel for power plants.

Acknowledgements

The authors gratefully acknowledge the Dutch technical foundation STW for generous financial support. We acknowledge the European Synchrotron Radiation Facility for provision of synchrotron radiation facilities. S.E.O. gratefully acknowledges long-standing collaborations with Profs. J. Sietsma and S. Van der Zwaag and Dr. N. Van Dijk of the Delft University of Technology and Prof. H. Poulsen, Drs. E. Lauridsen and S. Schmidt of the Danish Technical University, Risø National Laboratory, Dr. L. Margulies of the Brookhaven National Laboratory and Drs. J. Wright and G. Vaughan of the European Synchrotron Radiation Facility.

References

[1] T. Furuhara, T. Shinyoshi, G. Miyamoto, J. Yamaguchi, N. Sugita, N. Kimura, N. Takemura, T. Maki, Multiphase crystallography in the nucleation of intragranular ferrite on MnS plus V(C, N) complex precipitate in austenite, ISIJ International 43 (2003) 2028.
[2] Y. Ivanisenko, I. MacLaren, X. Sauvage, R.Z. Valiev, H.J. Fecht, Shear-induced alpha → gamma transformation in nanoscale Fe–C composite, Acta Materialia 54 (2006) 1659.
[3] W.T. Reynolds, S.S. Brenner, H.I. Aaronson, An Fim/Ap study of the Mo concentration within ferrite austenite interfaces in an Fe-0.88 at-percent C-1.06 at-percent Mo alloy, Scripta Metallurgica 22 (1988) 1343.
[4] E.V. Pereloma, I.B. Timokhina, M.K. Miller, P.D. Hodgson, Three-dimensional atom probe analysis of solute distribution in thermomechanically processed TRIP steels, Acta Materialia 55 (2007) 2587.
[5] Y. Adachi, K. Hakata, K. Tsuzaki, Crystallographic analysis of grain boundary Bcc-precipitates in a Ni–Cr alloy by FESEM/EBSD and TEM/Kikuchi line methods, in: International Conference on Recent Advances in Composite Materials (ICRACM 2004), Varanasi, India, Elsevier Science Sa, 2004, p. 252.
[6] H. Landheer, S.E. Offerman, R.H. Petrov, L.A.I. Kestens, The role of alpha/gamma orientation relationships during ferrite nucleation in an Fe–Cr–Ni alloy, Recrystallization and Grain Growth III 558–559 (Pts 1 and 2) (2007) 1413.
[7] A.F. Gourgues-Lorenzon, Application of electron backscatter diffraction to the study of phase transformations, International Materials Reviews 52 (2007) 65.

[8] W. Ludwig, S. Schmidt, E.M. Lauridsen, H.F. Poulsen, X-ray diffraction contrast tomography: A novel technique for three-dimensional grain mapping of polycrystals. I. Direct beam case, Journal of Applied Crystallography 41 (2008) 302.
[9] H.F. Poulsen, S. Garbe, T. Lorentzen, D.J. Jensen, F.W. Poulsen, N.H. Andersen, T. Frello, R. Feidenhansl, H. Graafsma, Applications of high-energy synchrotron radiation for structural studies of polycrystalline materials, Journal of Synchrotron Radiation 4 (1997) 147.
[10] H.F. Poulsen, S.F. Nielsen, E.M. Lauridsen, S. Schmidt, R.M. Suter, U. Lienert, L. Margulies, T. Lorentzen, D.J. Jensen, Three-dimensional maps of grain boundaries and the stress state of individual grains in polycrystals and powders, Journal of Applied Crystallography 34 (2001) 751.
[11] H.F. Poulsen, Three-Dimensional X-Ray Diffraction Microscopy-Mapping Polycrystals and Their Dynamics, Springer, Berlin, 2004.
[12] E.M. Lauridsen, S. Schmidt, R.M. Suter, H.F. Poulsen, Tracking: a method for structural characterization of grains in powders or polycrystals, Journal of Applied Crystallography 34 (2001) 744.
[13] S. Schmidt, S.F. Nielsen, C. Gundlach, L. Margulies, X. Huang, D.J. Jensen, Watching the growth of bulk grains during recrystallization of deformed metals, Science 305 (2004) 229.
[14] J. Banhart (Ed.), Advanced Tomographic Methods in Materials Research and Engineering, Oxford University Press, Oxford, 2008.
[15] L. Margulies, M.J. Kramer, R.W. McCallum, S. Kycia, D.R. Haeffner, J.C. Lang, A.I. Goldman, New high temperature furnace for structure refinement by powder diffraction in controlled atmospheres using synchrotron radiation, Review of Scientific Instruments 70 (1999) 3554.
[16] J.C. Labiche, O. Mathon, S. Pascarelli, M.A. Newton, G.G. Ferre, C. Curfs, G. Vaughan, A. Homs, D.F. Carreiras, The fast readout low noise camera as a versatile X-ray detector for time resolved dispersive extended X-ray absorption fine structure and diffraction studies of dynamic problems in materials science, chemistry, and catalysis, Review of Scientific Instruments 78 (2007) 091301.
[17] S.E. Offerman, Evolving microstructures in carbon steel, A neutron and synchrotron radiation study, PhD thesis, Delft University of Technology, Delft, 2003, p. 141.
[18] S.E. Offerman, N.H. van Dijk, J. Sietsma, S. Grigull, E.M. Lauridsen, L. Margulies, H.F. Poulsen, M.T. Rekveldt, S. van der Zwaag, Grain nucleation and growth during phase transformations, Science 298 (2002) 1003.
[19] S.E. Offerman, H. Sharma, Grain nucleation and growth of individual austenite and ferrite grains studied by 3DXRD microscopy at the ESRF, in: T. Kannengiesser, S.S. Babu, Y. Komizo, A.J. Ramirez (Eds.), In-situ Studies with Photons, Neutrons and Electrons Scattering, Springer-Verlag, Berlin, 2010, p. 41.
[20] J.W. Christian, The Theory of Transformations in Metals and Alloys, Pergamon Press, Oxford, 1981.
[21] T. Nagano, M. Enomoto, Calculation of the interfacial energies between alpha and gamma iron and equilibrium particle shape, Metallurgical and Materials Transactions A – Physical Metallurgy and Materials Science 37 (2006) 929.
[22] S.E. Offerman, Microstructures in 4D, Science 305 (2004) 190.
[23] S.E. Offerman, N.H. van Dijk, J. Sietsma, E.M. Lauridsen, L. Margulies, S. Grigull, H.F. Poulsen, S. van der Zwaag, Solid-state phase transformations involving solute partitioning: modeling and measuring on the level of individual grains, Acta Materialia 52 (2004) 4757.
[24] S.E. Offerman, N.H. van Dijk, J. Sietsma, S. van der Zwaag, E.M. Lauridsen, L. Margulies, S. Grigull, H.F. Poulsen, Reply to the discussion by Aaronson et al., to "Grain nucleation and growth during phase transformations" by S.E. Offerman et al., Science 298, 1003 (November 1, 2002), Scripta Materialia 51 (2004) 937.
[25] S.E. Offerman, N.H. van Dijk, J. Sietsma, E.M. Lauridsen, L. Margulies, S. Grigull, H.F. Poulsen, S. van der Zwaag, Phase transformations in steel studied by 3DXRD microscopy, Nuclear Instruments & Methods in Physics Research Section B – Beam Interactions with Materials and Atoms 246 (2006) 194.
[26] S.E. Offerman, H. Strandlund, N.H. van Dijk, J. Sietsma, E.M. Lauridsen, L. Margulies, H.F. Poulsen, J. Agren, S. van der Zwaag, Ferrite formation during slow continuous cooling in steel, Fundamentals of Deformation and Annealing 550 (2007) 357.
[27] C.E. Krill, L. Helfen, D. Michels, H. Natter, A. Fitch, O. Masson, R. Birringer, Size-dependent grain-growth kinetics observed in nanocrystalline Fe, Physical Review Letters 86 (2001) 842.
[28] S.E. Offerman, N.H. van Dijk, J. Sietsma, E.M. Lauridsen, L. Margulies, S. Grigull, H.F. Poulsen, S. van der Zwaag, Phase transformations in steel studied by 3DXRD microscopy, Nuclear Instruments & Methods in Physics Research Section B – Beam Interactions with Materials and Atoms 246 (2006) 194.
[29] D.J. Jensen, S.E. Offerman, J. Sietsma, 3DXRD characterization and modeling of solid-state transformation processes, MRS Bulletin 33 (2008) 621.
[30] W.F. Lange, M. Enomoto, H.I. Aaronson, The kinetics of ferrite nucleation at austenite grain-boundaries in Fe–C alloys, Metallurgical Transactions A – Physical Metallurgy and Materials Science 19 (1988) 427.
[31] P.J. Clemm, J.C. Fisher, The influence of grain boundaries on the nucleation of secondary phases, Acta Metallurgica 3 (1955) 70.
[32] W.F. Lange, M. Enomoto, H.I. Aaronson, The kinetics of ferrite nucleation at austenite grain-boundaries in Fe–C alloys, Metallurgical Transactions A – Physical Metallurgy and Materials Science 19 (1988) 427.
[33] E.M. Lauridsen, D.J. Jensen, H.F. Poulsen, U. Lienert, Kinetics of individual grains during recrystallization, Scripta Materialia 43 (2000) 561.
[34] C. Zener, Theory of growth of spherical precipitates from solid solution, Journal of Applied Physics 20 (1949) 950.
[35] W.M. Huang, M. Hillert, The role of grain corners in nucleation, Metallurgical and Materials Transactions A – Physical Metallurgy and Materials Science 27 (1996) 480.
[36] V.I. Savran, S.E. Offerman, J. Sietsma, Austenite nucleation and growth observed on the level of individual grains by three-dimensional X-ray diffraction microscopy, Metallurgical and Materials Transactions A – Physical Metallurgy and Materials Science 41A (2010) 583–591.
[37] http://www.npl.co.uk/advanced-materials/measurement-techniques/modelling/mtdata.
[38] V.I. Savran, Y. Van Leeuwen, D.N. Hanlon, C. Kwakernaak, W.G. Sloof, J. Sietsma, Microstructural features of austenite formation in C35 and C45 alloys, Metallurgical and Materials Transactions A – Physical Metallurgy and Materials Science 38 (2007) 946.
[39] G.R. Speich, V.A. Demarest, R.L. Miller, Formation of austenite during intercritical annealing of dual-phase steels, Metallurgical Transactions A – Physical Metallurgy and Materials Science 12 (1981) 1419.
[40] H. Sharma, A.C. Wattjes, M. Amirthalingam, T. Zuidwijk, N. Geerlofs, S.E. Offerman, Multipurpose furnace for *in situ* studies of polycrystalline materials using synchrotron radiation, Review of Scientific Instruments 80 (2009) 7.